



**European volcanological supersite in Iceland:  
a monitoring system and network for the future**

**Report**

**D5.1 - Automatic Interferograms and relative  
Earthquakes**

Work Package:	<i>Long-term magma tracking</i>
Work Package number:	<i>5</i>
Deliverable:	<i>Automatic Interferograms and relative earthquakes</i>
Deliverable number:	<i>5,1</i>
Type of Activity:	<i>RTD</i>
Responsible activity leader:	<i>Andy Hooper</i>
Responsible participant:	<i>University of Leeds</i>
Authors:	<i>K. S. Vogfjörd (IMO), K. Spaans (UoL), G.B. Guðmundsson (IMO)</i>

Type of Deliverable:	<i>Report</i>	<input checked="" type="checkbox"/>	<i>Demonstrator</i>	<input type="checkbox"/>
	<i>Prototype</i>	<input type="checkbox"/>	<i>Other</i>	<input type="checkbox"/>
Dissemination level:	<i>Public</i>	<input checked="" type="checkbox"/>	<i>Restricted Designated Group</i>	<input type="checkbox"/>
	<i>Prog. Participants (FP7)</i>	<input type="checkbox"/>	<i>Confidential (consortium)</i>	<input type="checkbox"/>

**Seventh Framework Programme  
EC project number: 308377**



## Summary

This deliverable summarizes results from developments of automatic processing of interferograms and relative relocations.

### **Automatic Interferograms**

An algorithm has been developed capable of ingesting radar data, and producing deformation maps within hours. This is achieved by splitting the most time consuming step, the coherence (a measure of signal-to-noise ratio) estimation, in two. For each pixel, previously acquired data are used to estimate neighbourhood points that, on average, behave similarly. This information is stored, to be used when a new image comes in. For each interferometric combination made with this new image, the phase and amplitude of each pixel are compared to the identified similar neighbourhood pixels, yielding an estimate for the coherence. By taking the time consuming step of identifying similar pixels out of the near-real-time processing chain, the processing time is significantly reduced. Another benefit of this two-staged approach is that each new interferometric combination can be processed completely independently, allowing for great flexibility in terms of parallelization of the computations.

The coherence estimate is first used to select points with sufficient signal-to-noise ratio, and secondly as input into the phase-unwrapping algorithm. The phase-unwrapping process turns the cyclic interferometric phase signal into a continuous deformation map, which is the final output of the algorithm.

### **Automatic Relative Relocations**

An automatic, relative earthquake relocation algorithm (*ARL*), which was previously developed and operated to map active faults in the South Iceland Seismic Zone has been adapted and implemented for the Bárðarbunga dyke intrusion. The algorithm is operating in test mode, but is already returning good-to high-precision earthquake locations within 20 minutes of their occurrence in the Bárðarbunga intrusion dyke. The process relies on the existence of enough previously relatively located events, to form a library of high-quality event locations for comparison with each new event that fulfils a predefined quality criterion. At Bárðarbunga, this library presently includes 3554 selected events, well distributed on the intrusion dyke, both horizontally and vertically, as well as in magnitude. As more events at Bárðarbunga are relatively relocated, the library will grow in number and expand to encompass a wider region of the volcanic system. The input parameters of the system and the set-up are still being tuned for optimum and faster results. When fully tested and developed, the process is expected to return automatic, high-precision earthquake locations in the Bárðarbunga volcanic system in near-real time.

## Contents

Summary	1
Contents	2
1. Automatic Interferograms	3
1.1. Introduction	3
1.2. Rapid InSAR processing	3
1.2.1. InSAR background	3
1.2.2. Algorithm overview	5
1.2.3. Eyjafjallajökull test case	6
1.3. References	9
2. Automatic Relative Relocation of Earthquakes	11
2.1. Introduction	11
2.2. Relative earthquake locations and library events	13
2.3. Automatic earthquake locations – <i>ARL</i>	14
2.4. Conclusions	19
2.5. Acknowledgements	20
2.6. References	20

# **1. Automatic Interferograms**

## **1.1 Introduction**

Radar interferometry is a differencing technique, capable of measuring Earth surface deformations with cm to mm accuracy. The technique is widely used for geophysical applications like tectonic and volcanic activity. Current satellites acquire more data and have faster repeat cycles, allowing radar interferometry to potentially be used as a monitoring tool, but only if the data can be processed fast.

Interferometric Synthetic Aperture Radar (InSAR) has over the last two decades proven itself to be a valuable measurement technique to track magma movements at volcanic systems, see e.g. *Hooper et al. [2011]* and *Sigmundsson et al. [2010]*. In recent years, the data availability has greatly increased, and will increase further now that the European Space Agency's Sentinel-1 satellite has started to acquire data. To fully take advantage of this large data volume, an automatic, fast processing chain is required. This allows monitoring of volcanic systems, independent of their location, and provide timely information to civic authorities and scientists on the ground in time of crises. This section gives an overview of the developed system, and demonstrate its capabilities.

## **1.2 Rapid InSAR processing**

### 1.2.1 InSAR background

InSAR is a radar signal differencing technique, which uses two high resolution radar images taken from the practically the same position at different points in time to infer surface deformations. As the radar signal can only range in the direction of its Line-of-Sight (LOS), it is most sensitive to movements in this direction, and insensitive to movements perpendicular to it. It is also an opportunistic technique, in that it relies on scattering properties of the Earth surface to reflect the radar signal back to the satellite. If between acquisitions the scattering properties of a resolution element changes, or the position of the satellite at the two times of acquisition is too different, the change in scattering of the signal creates a noise component (Fig. 1.1). This phenomenon is known as decorrelation (Zebker and Villasenor [1992]), and is one of the main challenges in InSAR processing.

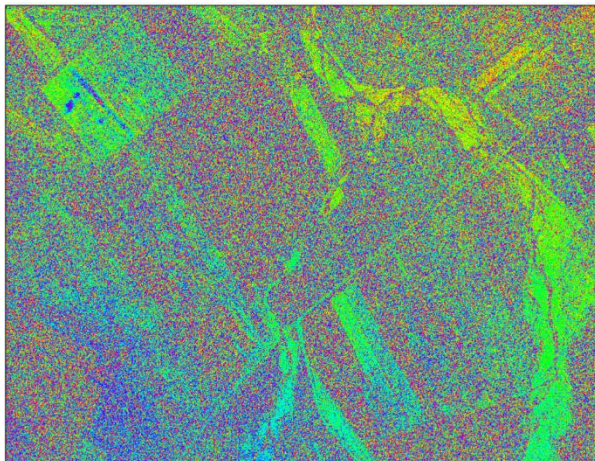


Figure 1.1: Interferogram showing a mix of signal and decorrelation noise. In this case, the noise is mostly caused by agricultural fields changing over time.

Coherence is a measure of decorrelation, where a coherence of 1 represents no decorrelation, and 0 means full decorrelation. The complex coherence  $\varphi_c$  is defined as:

$$\varphi_c = \frac{E(M \cdot \bar{S})}{\sqrt{E(M \cdot \bar{M}) \cdot E(S \cdot \bar{S})}}$$

Where  $E()$  is the expectation,  $M$  is the master image,  $S$  is the slave image and the overbar represents the complex conjugate. The coherence is the absolute value of the complex coherence. The coherence for each point can be estimated using:

$$\varphi = \frac{\frac{1}{N} \sum_{i=0}^N M_i \cdot \bar{S}_i}{\sqrt{\frac{1}{N} \sum_{i=0}^N M_i \cdot \bar{M}_i \cdot \frac{1}{N} \sum_{i=0}^N S_i \cdot \bar{S}_i}}$$

Where  $N$  is a number of pixels surrounding the current point. Most commonly, these surrounding pixels are in a rectangular window around the point, a method referred to as the boxcar method. This method suffers from two main drawbacks: Firstly, because of the moving window, the coherence estimate is spatially correlated, and thus tends to smear out features, leading to a loss of resolution. Secondly, for fully decorrelated areas, erroneously high coherence estimates occur due to areas having similar values by chance, leading to a noisy looking coherence estimate and a lack of contrast between decorrelated areas and areas with low coherence, but some signal. Figure 1.2 shows an example of a boxcar coherence estimate, showcasing these two limitations.

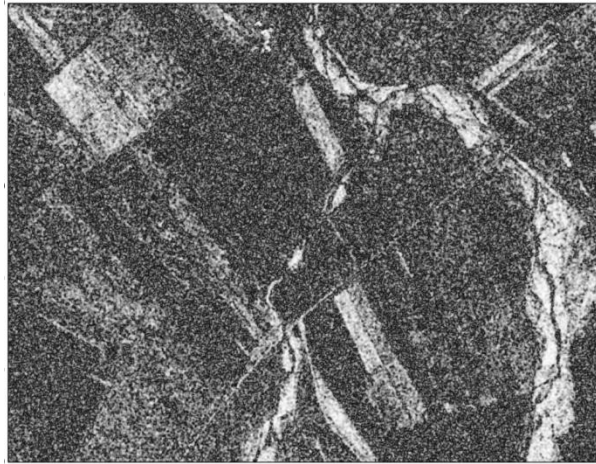


Figure 1.2: Boxcar coherence estimate for the interferogram shown in Fig. 1.1. The speckly noise due to erroneously high coherence estimates is clearly visible, as is the loss of resolution over the smaller roads and barriers in between fields.

These coherence estimates are necessary to select coherent points, and as input into phase unwrapping algorithms. Phase unwrapping is the process of estimating continuous deformation maps from the periodic InSAR phase measurements. While the boxcar method is the only option to estimate the coherence for single interferograms, the limitations of the method means it could only be applied to high quality interferograms, making much of the data unusable.

Timeseries methods were developed to enhance our ability to use InSAR data. These methods require a set of interferograms taken from the same viewing geometry, and use the time dimension to estimate the coherence of each pixel. Broadly speaking, timeseries methods can be split into two categories, the Persistent Scatterer (PS) (Ferretti et al. [2001], Hooper et al. [2007]) and the Small Baseline (SB) (Berardino et al. [2002], Hooper [2008]) methods. These methods focus on different types of points with stable scattering behaviour through time, and selecting the phase values of just these points. This leads to the same points being selected in every interferogram. Although this results in overall a high quality timeseries of measurements, it does lead to a loss of information and noisy points being selected in some of the lower quality interferograms, as will be discussed later.

A relatively recent development in InSAR processing is to identify for each pixel neighbouring pixels that on average throughout the dataset behave in a similar manner (Ferretti [2011]), which we refer to as cousins. These cousins tend to belong to the same type of scattering surface, e.g. buildings, fields, roads, etc. One of the applications of these cousins is that they can be used to estimate the coherence of the point in question, using Eq. 2. Using cousins reduces the problems with loss of resolution and erroneously high coherence estimates for decorrelated points.

### 1.2.2 Algorithm overview

We have developed a two stage algorithm that can rapidly ingest new images, and forms unwrapped interferometric combinations with them. Our algorithm

uses cousins to calculate the coherence, and a two stage selection procedure to maximise the information extracted from the interferograms.

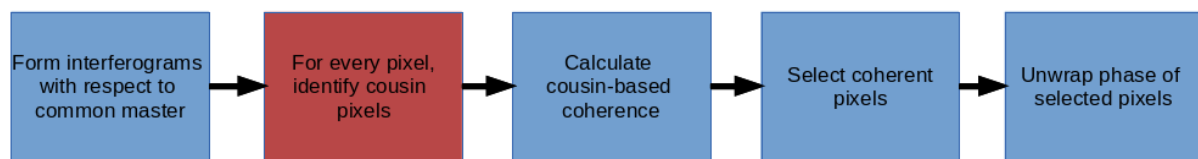


Figure 1.3 High-level overview of the processing workflow. To save time, the red processing step is on performed on an initial set of interferograms, not on newly incoming images.

Fig. 1.3 shows a flow chart describing the general workflow of the algorithm. We start with an initial dataset, for which we form for each image the interferogram with respect to a common master. From this, we can make all possible interferometric combinations. We use this initial dataset to identify the cousins for each point.

Given that cousins are not expected to change rapidly through time, we do not re-estimate them for each new image coming in. We save the cousin information estimated on the initial dataset, and when a new image comes in, we form the interferometric combinations with respect to that image, and continue with the remainder of the workflow. This prevents us from having to re-analyse the entire dataset every time we want to include a new image, as would be the case with the PS or SB methods. The remainder of the processing chain is independent for each interferogram, leading to far greater flexibility in parallelizing the algorithm implementation.

The cousin information is used to estimate the coherence. Once the coherence estimate is obtained, we select points by setting a threshold on the coherence. Even though the problem of erroneously high coherence estimates in fully decorrelated areas is mitigated significantly by using the Cousin Coherence method compared to the Boxcar method, it still persists, and leads to a high threshold being necessary. We solve this by selecting points on the multilooked interferogram as well. Multilooking is the process of averaging several pixels, to form a lower resolution image. The advantage is that this works as a filter, reducing the noise. For the coherence map, this means that for fully decorrelated areas, the occasional isolated outlier will be counteracted by the surrounding low coherence points. For areas with low, but some coherence, the spatial correlation of these points will reinforce them. This creates enough contrast between the two situations to select the vast majority of the signal, and minimize the falsely selected points. The selected points, together with their estimated coherences, are used in the phase unwrapping algorithm (Chen and Zebker [2002]).

### 1.2.3 Eyjafjallajökull testcase

We use data collected before and during the 2010 Eyjafjallajökull eruption to demonstrate the algorithm and its effectiveness. Although our method is faster than traditional time series methods, we demonstrate here that the performance of our method in terms of the quality of selected points is often better. To

evaluate the performance of the point selection procedure, we compare results obtained using our method with results obtained using a widely used Small Baseline time series method (Hooper 2008). We processed the full dataset of 29 images, and compare the performance of the selection algorithm for four different interferograms of differing quality.

Fig. 1.4 shows the selection process for a high coherence interferogram in the dataset. The cousin coherence selection extracts far more information from the full interferogram than the Small Baseline method does. The main reason for this is that the Small Baseline method selects 1 set of points for all interferogram, while the Cousin coherence method selects a set of points for each interferogram individually. This means that images with poorer coherence influence the overall point selection of the Small Baseline method.

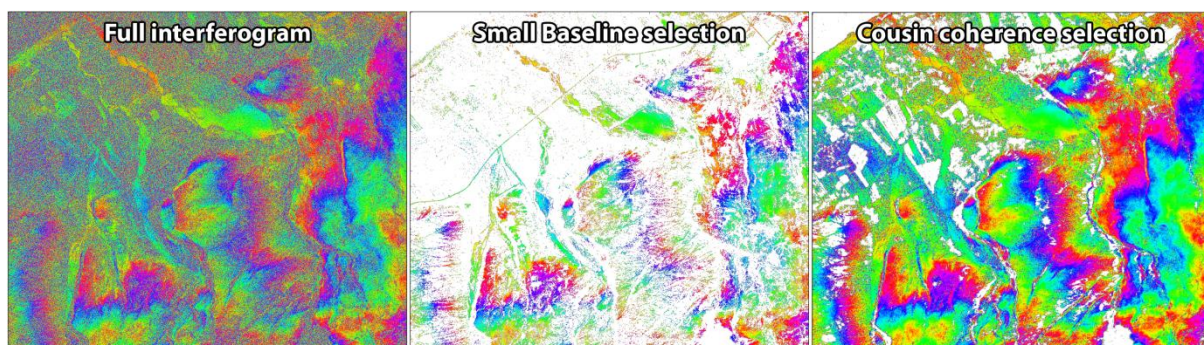


Figure 1.4: Demonstration of point selection in a high coherence interferogram (20090618-20090629): Full interferogram (left), point selection using Small Baseline method (middle) and cousin coherence selection (right).

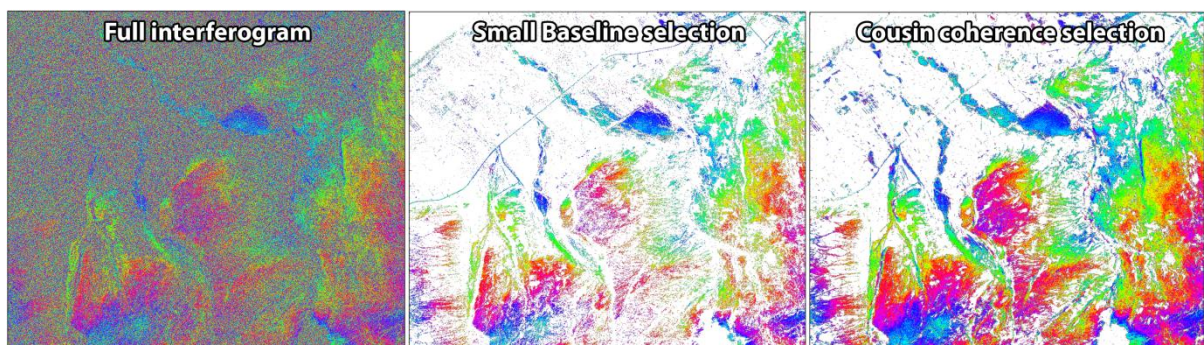


Figure 1.5: Demonstration of point selection in a medium coherence interferogram (20090618-20090903): Full interferogram (left), point selection using Small Baseline method (middle) and out cousin coherence selection (right).

An example of a lower coherence image is given in Fig. 1.5. The decorrelation here is caused by the longer temporal baseline (the time period between the acquisitions of the two images). In this case, the time between acquisitions is close to three months, which causes the agricultural fields in the top left of the image to decorrelate. For the Small Baseline method, the loss of coherence in the fields in this and similar images, which make up the majority of images in the dataset, causes the loss of information in the same area in high coherence images. As the fields are decorrelated, our method also selects few points in the area. However, higher on the flanks of the volcano, we also see a difference in

point selection. Our method selects significantly more points on the flanks of the volcano.



Figure 1.6: Demonstration of point selection in an interferogram affected by snow (20100204-20100331): Full interferogram (left), point selection using Small Baseline method (middle) and cousin coherence selection (right).

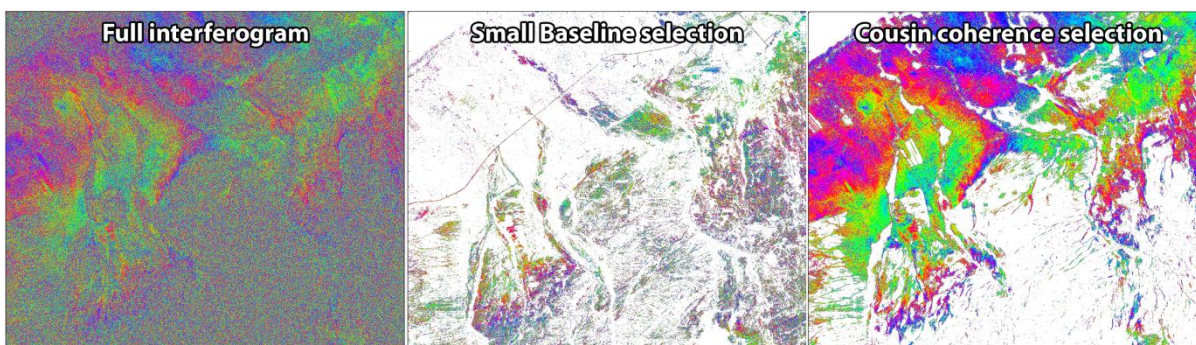


Figure 1.7: Demonstration of point selection in an interferogram affected by ash (20100204-20100331): Full interferogram (left), point selection using Small Baseline method (middle) and cousin coherence selection (right).

The reason that for the scene shown in Fig. 1.5 less points are selected on the volcano flank by the Small Baseline method is shown in Fig. 1.6 and 1.7. From the full interferograms, we see that the flanks are almost completely decorrelated, caused by snow (Fig. 1.6) and ash (Fig. 1.7). The decorrelation mechanism for Fig. 1.6 and 1.7 is different than that of Fig. 1.5, leading to different areas being affected. As discussed above, decorrelation in images with lower coherence affects the points selected using the Small Baseline method, leading to coherent points in high coherence images being rejected, resulting in a loss of information. Another issue with the Small Baseline method can be seen in both Fig. 1.6 and 1.7: Many of the selected points by the method are actually decorrelated, leading to a very noisy result. Indeed, our method selects a very low number of points higher up on the flanks, due to the high number of decorrelated pixels there. Reversely, on the lower lying fields, which are less affected by snow and ash, we select far more points, and manage to extract the signal present in the full interferogram, while reducing the noise dramatically.

Figures 1.4 to 1.7 demonstrate the advantage our selection method has compared to traditional time series methods. The compromise that has to be made by these other methods is not necessary using our method, due to the

individual coherence estimate. This maximizes the information that is extracted from the timeseries, while minimizing the noise.

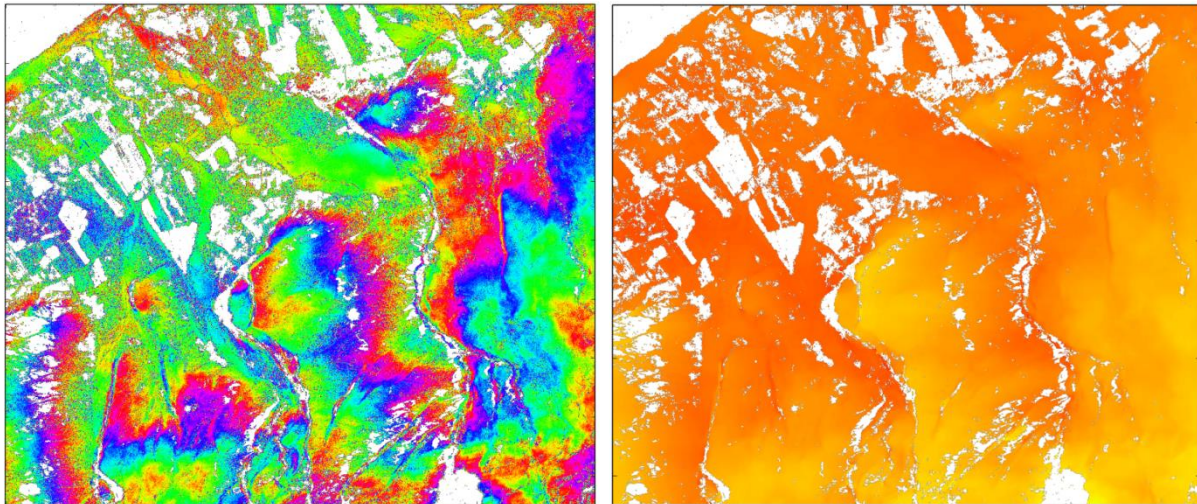


Figure 1.8: Comparison between the wrapped (left) and unwrapped phase.

The high signal-to-noise ratio and spatial sampling of the points selected in the interferograms greatly aid unwrapping. Fig. 1.8 shows an example of the unwrapping result.

The flexibility offered by our method, in particular by being able to process images individually, results in a large reduction of processing time. For traditional timeseries methods, and for the Small Baseline method in particular, it can take several days of processing time to obtain results. Using our method, we can obtain unwrapped interferograms within hours after receiving a new image, with intermediate results being much faster.

### 1.3 References

Berardino, P. et al, 2002. A new algorithm for surface deformation monitoring based on small baseline differential SAR interferograms. *IEEE transactions on Geoscience and Remote Sensing*, 40, p2375-2383.

Chen, C.W. & Zebker, H.A., 2002. Phase unwrapping for large SAR interferograms: Statistical segmentation and generalized network models. *IEEE Transactions on Geoscience and Remote Sensing*, 40, p1709-1719.

Ferretti, A., Prati, C. & Rocca, F., 2001. Permanent scatterers in SAR interferometry. *IEEE transactions on Geoscience and Remote Sensing*, 39, p8-20.

Ferretti, A. et al, 2011. A New Algorithm for Processing Interferometric Data-Stacks: SqueeSAR. *IEEE transactions on Geoscience and Remote Sensing*, 49, p3460-3470.

Hooper, A., Segall, P. & Zebker, H., 2007. Persistent scatterer interferometric synthetic aperture radar for crustal deformation analysis, with application to Volcán Alcedo, Galápagos. *Journal of Geophysical Research*, 112, B07407.

Hooper, A., 2008. A multi-temporal InSAR method incorporating both persistent scatterer and small baseline approaches. *Geophysical Research Letters*, 35, L16302.

Hooper, A. et al., 2011. Increased capture of magma in the crust promoted by ice-cap retreat in Iceland. *Nature Geoscience*, 4, p783-786.

Sigmundsson, F. et al, 2010. Intrusion triggering of the 2010 Eyjafjallajökull explosive eruption. *Nature*, 486, p426-430.

Zebker, H.A. & Villasenor, J., 1992. Decorrelation in interferometric radar echoes. *IEEE transactions on Geoscience and Remote Sensing*, 30, p950-959.

## 2. Automatic Relative Relocation of Earthquakes

### 2.1 Introduction

All events recorded by the Icelandic seismic monitoring system, SIL are automatically located and their magnitude estimated within 2 minutes of their origin time (OT). These locations are sometimes determined by only a few phase detections (P- and S-phases) and thus the location accuracy may be less than optimal. A measure of this accuracy is the system's internal quality constant. All events are later manually reviewed, where arrivals are adjusted, polarities added and magnitudes recalculated (Stefánsson et al., 1993; Böðvarsson et al, 1996; 1999). Depending on the activity rate, the time between automatic and reviewed location can be as short as minutes or as long as months to years. For example, a year after the onset of the Bárðarbunga unrest, roughly 60% of the events automatically detected in the first 25 days of the episode have yet to be manually revised, and on three of these days this ratio is around 90%.

At Bárðarbunga, the detection threshold for microearthquakes has been improving over the last decade, but before FUTUREVOLC, most stations were located outside the Vatnajökull glacier. One of the goals of the project was to improve seismic detection at volcanoes in Vatnajökull, in particular Bárðarbunga and Grímsvötn. This was achieved by adding 4 continuously transmitting stations inside the glacier; *hus* and *ksk* on rock outcrops (nunataks) in the glacier, and *djk* and *bjk* in the ice itself. Furthermore two seismic arrays, *jok* and *iey* were installed (under WP6) west of the glacier and two temporary sites at *von* and *hae*. At the onset of the Bárðarbunga unrest in 2014, several more transmitting stations were temporarily added (*ham*, *kve*, *urh*, *tho*, *bar*; *urh* is also part of a third, temporary seismic array). [Figure 2.1](#) shows the station density at the end of 2014, where broadband stations are shown in red. The improved seismic detection provided by the greater station density has enabled the additional implementation of an automatic relative relocation procedure for the Bárðarbunga volcanic system.

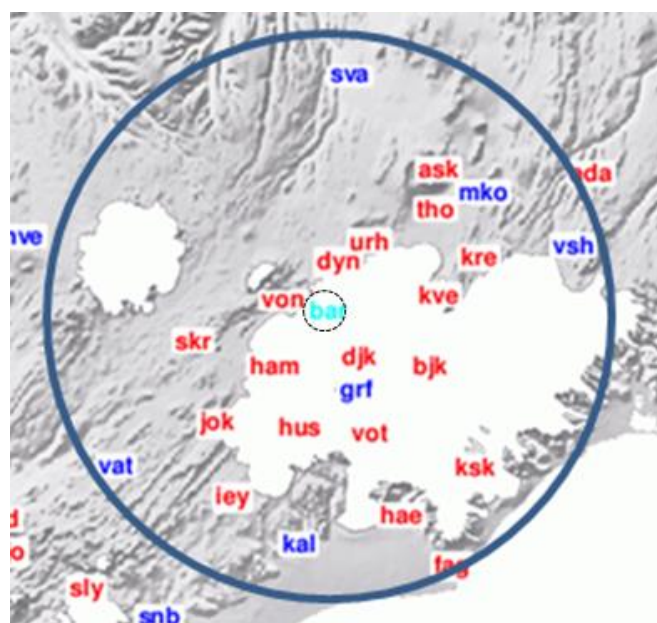
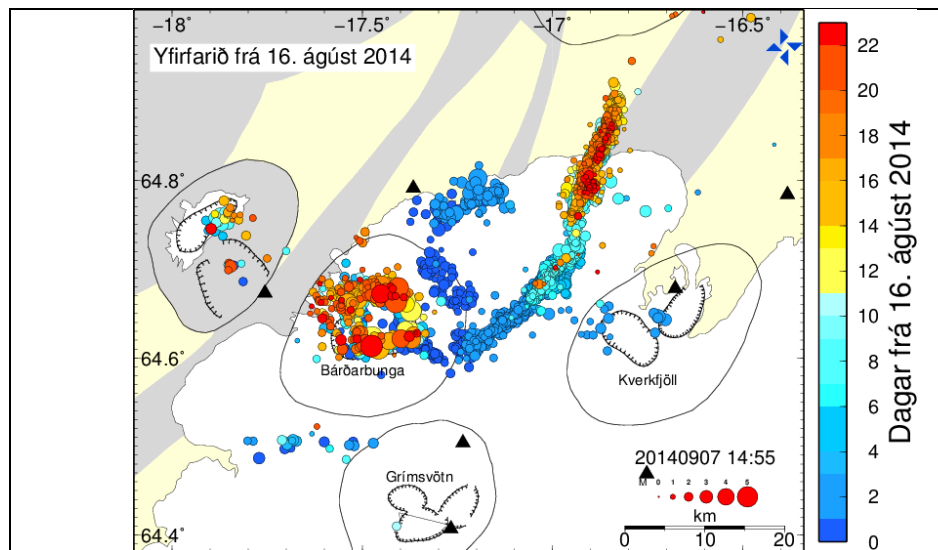


Figure 2.1. Map showing seismic stations in and around Vatnajökull glacier. Bárðarbunga is in the center of the figure, with the caldera rim roughly sketched (dashed). Broadband stations are shown in red, short period in blue. One strong motion station is located inside the Bárðarbunga caldera (light blue). The 95 km distance from Bárðarbunga is drawn with a dark blue circle.

As previously mentioned, monitoring and tracking seismic activity during extended swarms suffers from delayed revision and relocation of the initial automatic locations and therefore limits the level of interpretation that can be achieved during the episode. Figure 2.2a shows the manually revised events 23 days into the unrest, representing only around 20% of all the detected events. To improve the accuracy and timeliness of revised earthquake locations, at Bárðarbunga the goal in this deliverable is to develop an automatic process to generate high-precision earthquake relocations in near-real time. The procedure, which applies relative earthquake relocations using cross-correlated waveforms, is an adaptation of Slunga's et al. (1995) original relative relocation method. The process is expected to ensure consistent access to high-quality relocations within minutes of an earthquake, thus improving the monitoring of volcanic unrest, while at the same time decreasing the time spent on manual revisions once they are finally performed.

The new automatic relocation process starts with the locations available from the routine automatic system after 2 minutes and to operate, needs a library of older events to compare with each new event. The library contains previous relatively relocated events, well distributed in space and covering the required range of magnitudes. Part of the preparatory work for establishing the process therefore requires extensive relative relocations of older earthquakes.



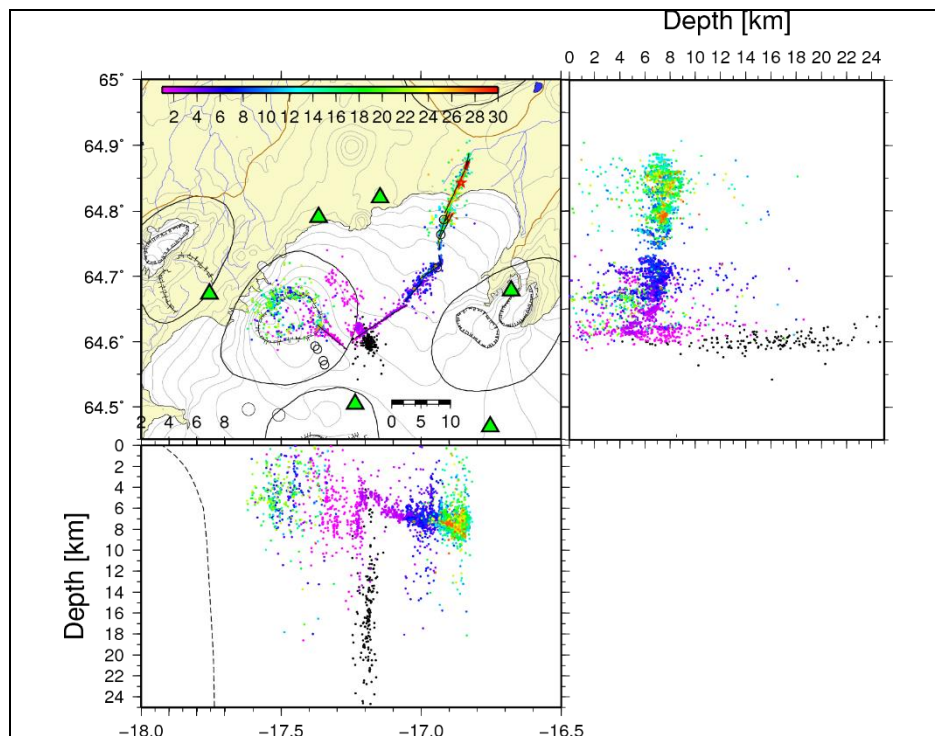


Figure 2.2. Event locations from the first 3 weeks of the Bárðarbunga unrest. (Upper) 5300 manually revised earthquake locations during the first 23 days of the Bárðarbunga unrest episode, starting 16 August 2014. The events, which are color coded according to time represent only about 20% of all the automatically detected events. (Lower) ~4000 relatively relocated events at Bárðarbunga during the first 28 days of the unrest, starting at 16 August 2014. The events are color coded according to time of occurrence.

## 2.2 Relative earthquake locations and library events

The relative relocations are obtained through the double-difference method of Slunga et al. (1995) based on minimizing the differences between observed and theoretically calculated waveform travel times from different events at each station. Such relocation methods have been developed by other researchers (Got et al., 1994; Waldhauser and Ellsworth, 2000; 2002) and widely applied in other regions. The Slunga method applies iterative inversion of the weighted square sums of: absolute (manually picked) P- and S arrival time differences, as well as the double differences of (i) absolute arrival times of P- and S-waves, (ii) relative arrival times of P- and S-waves and (iii) relative S-P arrival times. The double differencing minimizes the effects of inadequacies in the velocity model used, which for the Bárðarbunga relocations is the standard 1D velocity model, SIL (Stefánsson et al., 1993). This model is also used by the SIL routine analysis system.

Thousands of microearthquakes at Bárðarbunga recorded by the SIL digital network over the past twenty years have already been relatively relocated (Vogfjörd et al., 1999, 2011, 2015a, 2015b, 2015c; Sigmundsson et al., 2015) using the Slunga et al. (1995) relative relocation method. The first decade of this period however, does not result in many high-quality locations due the sparse

seismic station coverage of that time, but over the latter decade, the network coverage has been constantly improving, thus providing tighter constraints on the event locations. Due to the greatly improved station density in 2013 and 2014, the events recorded during the Bárðarbunga unrest episode in 2014/2015 have provided the best relocated events and are therefore selected for the initial event library to be used in the automatic relocations (Figure 2.2b). In this data set, each event is inverted in a group with 43 of its nearest neighbors and overlap of groups is enough to ensure that most events are located in at least 5 groups. The average location from these 5 groups is then the final relocation of the event. The events generated by the propagating dyke intrusion from 16 August to 12 September 2014 have the highest accuracy of all recorded events in the Bárðarbunga system and resulted in the detailed definition of the segmented intrusion dyke, where *rms* deviations of the relative locations from the segmented planes was only around 100 m (Sigmundsson et al., 2015) (Figure 2.3). From this data set 3554 well distributed events (in location and magnitude) were selected for the initial event library for the dyke intrusion. More events from the dyke and caldera will be added in the coming months.

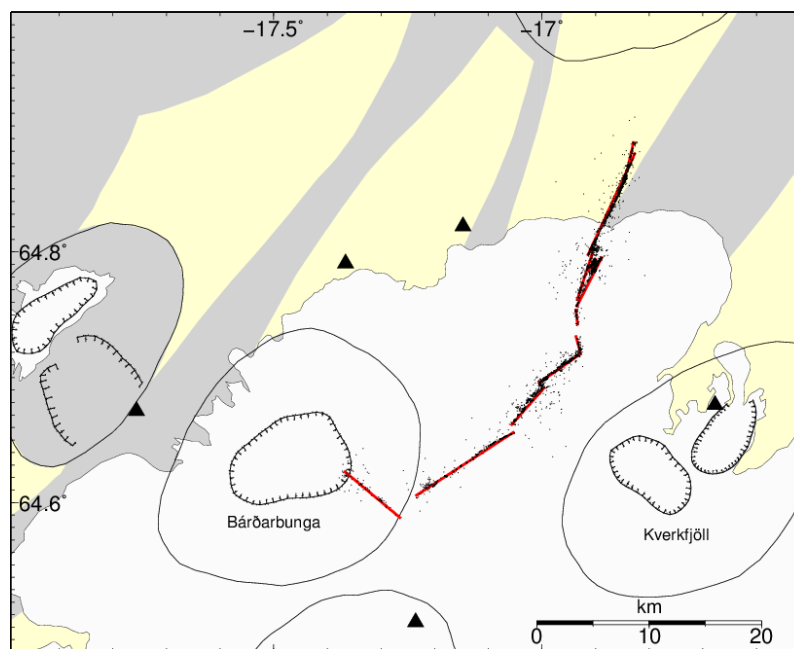


Figure 2.3. Relative locations of 4 thousand events defining the 8 segments of the Bárðarbunga dyke intrusion. A selection from these locations forms the initial event library used in the ARL process. The dyke segments are shown by red lines. All relocated events are shown, (good and bad).

## 2.3 Automatic relative locations – ARL

The aim is to implement automatic, near-real-time, relative relocation of seismicity (ARL) to monitor activity at Bárðarbunga, using waveforms from the previously mapped high-precision events (library events) to correlate with waveforms from the newly detected events passing a certain quality level. As

previously mentioned, the single-event, automatic locations are available from the SIL analysis system within 2 minutes of the origin time (OT) with a location accuracy on the order of one km in latitude and longitude, but uncertainty in depth is greater and also more affected by velocity model; depth uncertainty is estimated to be up to several km. Manual revision of the automatic locations generally improve accuracy to become within a few hundred meters in latitude and longitude and 1-3 km in depth (Böðvarsson et al, 1999). These however, can take a long time to complete and therefore may not be available to evaluate and track activity in near-real time when activity is high. Location accuracy of relatively located events can be much better, on the order of tens of meters at best, depending on the availability and quality of data and appropriateness of the velocity model used to approximate the crustal structure (Slunga et al., 1995). Automatic, near-real time generation of relative relocations can therefore enable faster and higher-precision mapping of the activity at Bárðarbunga than manual revision can.

An initial version of the *ARL* algorithm was originally developed and operated to map active faults in the South Iceland Seismic Zone and was tested in the Hengill region, where it gave good results within 5 minutes of an event (Vogfjörð et al., 2010). Its adaptation to operate at Bárðarbunga involves – in addition to the generation of a high quality event library – further development of the algorithm and the addition of a depth dependency, due to the much greater depth range of events at Bárðarbunga than at Hengill volcano. The new process was implemented at the Bárðarbunga dyke intrusion on 19 May 2015, which was marked by delivery of Milestone *MS33*. Since then, the process has been operating in test mode, while the library is being improved as more quality relative locations become available and while parameters are being adjusted for optimum and faster results.

New, automatic events above a certain quality threshold are passed to the algorithm, where they are correlated with a subset from the library (sub-library), containing the closest events to the new earthquake. If the number of events in the sub-library exceeds a maximum number ( $N_{max}$ ), then the events are further selected according to magnitude limits and, for certain areas, according to depth limits. In the present setup, when an event occurs, 200 library events within 4 km distance are selected and their waveforms correlated with the new event. The 39 library events correlating best with the new event are then chosen for a final inversion for relative location. The algorithm starts after a certain time delay (specified by  $OT+T_d$ ), presently every 14 minutes, and twice if more than one new event have occurred during that time. In its present state, the location process takes 12–14 minutes; 10–13 minutes to correlate the waveforms and 2 minutes to invert the relative travel times. The parameters that need to be set are shown in [Table 2.1](#) and the procedure is as follows:

- When a new event with a quality above a certain limit ( $Q_{min}$ , in Table 1) is detected within the test area, library events within distance  $r$  are selected and stored in a temporary sub-library.
- If needed, the number of sub-library events is reduced to a maximum number ( $N_{max}$ ) to limit processing time to a few minutes.
- If events in the same area have recently ( $T_{recent}$ ) been automatically relocated, then they are also added to the sub-library.

- Waveforms of the new event are correlated with the selected waveforms from the sub-library at stations within  $D_{max}$  distance to measure relative times.
- Finally the relative times from the 40 best correlating events are chosen for inversion to obtain a relative location for the new event.
- The procedure searches for new events every ( $T_{int}$ ) minutes and starts processing if events are found. Immediately after the process finishes, it runs a second time, in case more events occurred during the processing time.

Table 2.1. Parameter values used in the ARL procedure at Bárðarbunga.

Parameter	Value	Description
$Q_{min}$	10	Required Minimum Quality <sup>1)</sup> of event
$r$	4 km	Distance from the automatic location, within which a sub-library is selected
$N_{max}$	200	maximum number of sub-library events
$N_{min}$	60	minimum number of sub-library events
$N_{rec}$	20	Maximum number of newly located events in a sub-library
$D_{max}$	50 km	Maximum distance from automatic location to station
$S_{max}$	20	Maximum number of stations used in relocation
$T_{recent}$	30 days	Recent time in days from which new events are added to the sub-library
$T_{int}$	14 minutes	Time between checking for new automatic events
$T_d$	2 minutes	Wait time after origin time to start process

<sup>1)</sup> This is the internal quality measure of the location accuracy and consistency in the automatic P- and S-arrival picks of the automatic SIL system, where a value of 99 is the highest quality and events with quality lower than 10 are not entered into the catalogue unless they are in an area of ongoing swarms.

Table 2.1 shows that during the test period in May/June 2015 the ARL process was run every 14 minutes. This rather long delay time depends on the total processing time, which is predominantly due to delays in accessing the waveform data for correlation; the inversion takes only 1-2 minutes. The delays are caused by recent changes made at IMO. During 2014, the whole operational environment of the SIL system underwent major changes, when the automatic processing was moved to virtual machines, where it is now operating. Previous tests before the move, of the older ARL versions in the Hengill region were, for example, run every 5 minutes, when processing time was only 3-5 minutes for each event (Vogfjörd et al., 2010). The present access delays are expected to be improved in the near future, at which time it should be possible activate the process every 5 minutes or less.

ARL location results for the Bárðarbunga dyke over the period 19 May to 12 June 2015, are shown in Figure 2.4. During this time 203 events were automatically detected in the dyke area. Of those, 134 events (black circles), or 66% passed the quality criterion to enter the ARL process, where their waveforms were correlated with waveforms from the library events (grey crosses). The resulting ARL locations are shown with colored squares, where color coding represents location quality. The best locations, those with over 50 correlations, are shown in red, adequate locations, those with over 30 correlations in blue and the rest in black. Through the relocation, the events move within 2 km in latitude and

longitude. The change in depth can be much greater, up to 8 km, but is most often within 2 km. The results show that the best ARL locations (red and blue squares) concentrate near or on the dyke. The ones with fewer constraints (correlations) can drift away from the library clusters along the dyke. The greater deviation of ARL events at the southern end of the dyke reflects the missing deeper events from the library. These events, as well as caldera events will be added to the library.

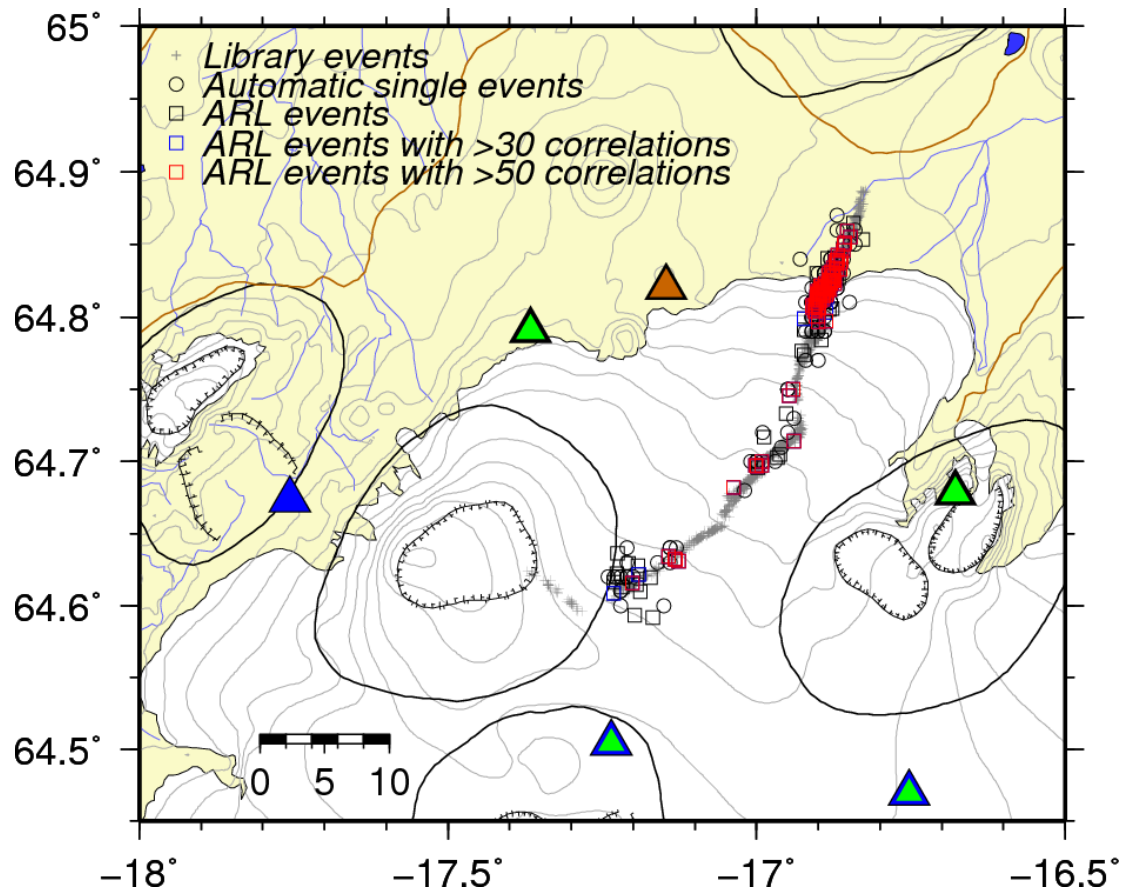


Figure 2.4. Location results from the first month of ARL operation at Bárðarbunga, between 19 May and 12 June 2015, when 134 events were passed to the process. The Library events along the dyke intrusion are shown with grey crosses, while routine automatic locations are shown with black circles and ARL locations with squares. Good ARL locations, with >50 correlating waveforms are red, adequate locations, with >30 correlations in blue and less constrained locations in black. Seismic stations are shown with triangles.

The quality distribution of ARL locations is displayed in [Figure 2.5](#), which shows how well constrained the locations of the 134 events are. 67% of the events relocated with the ARL algorithm (44% of all located events) are well constrained, with 50 P- and S-waveform correlations and 72% of the events (48% of all located events) are adequately constrained with 30 waveform correlations. As more events representing the full range of events from the dyke and the caldera are added to the library the quality of the locations is expected to increase.

### Bardarbunga (dyke)

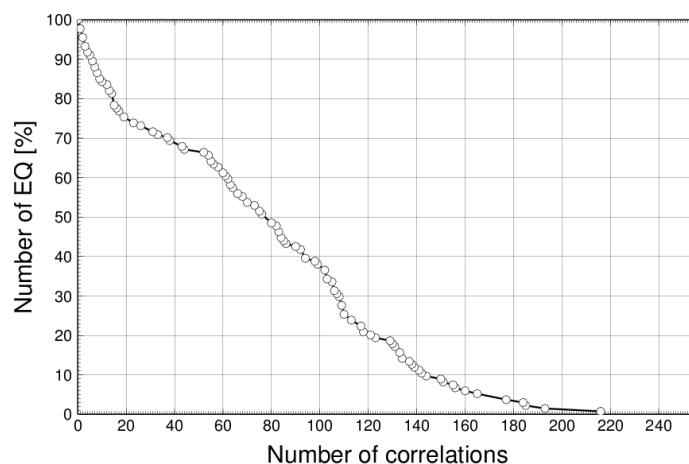
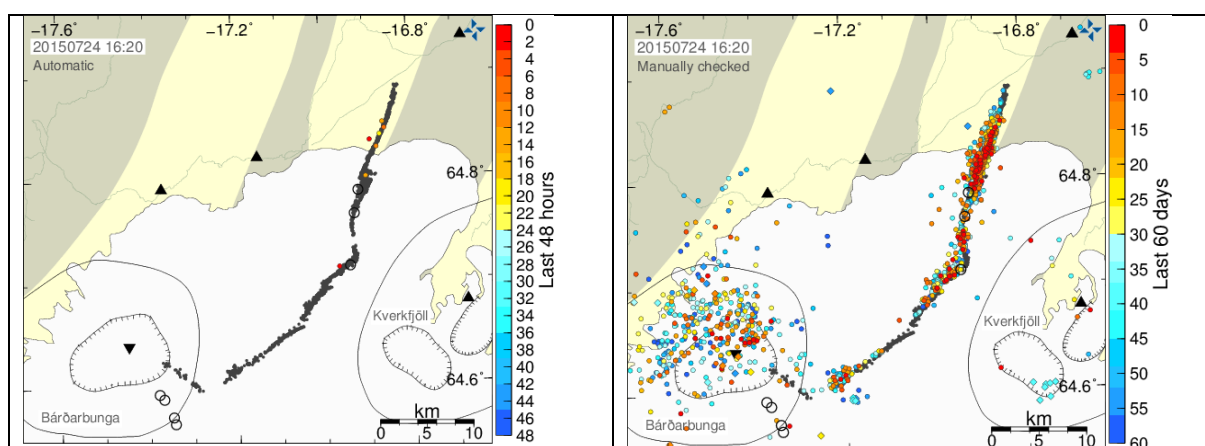


Figure 2.5. Statistics of the 134 ARL locations processed during the first month of operation, from 19 May to 12 June 2015, showing number of correlations vs percentage of earthquakes located. 72% of the events that passed to the ARL process have adequate location accuracy, with over 30 (P and S) correlations and 67% are well located with over 50 correlations.

A script to automatically generate real-time GMT maps of the original event locations together the improved ARL locations has been written and activated to show the location results on IMO’s web site, at: <http://hraun.vedur.is/ja/FUTUREVOLC/BB>. A screen shot of the display from 24 July 2015 is shown in Figure 2.6. The display shows four maps: the last 48 hours of (1) routine, automatic, single-event locations, and (2) ARL locations, as well as the last 2 months of (3) reviewed routine, single-event locations and (4) ARL locations.



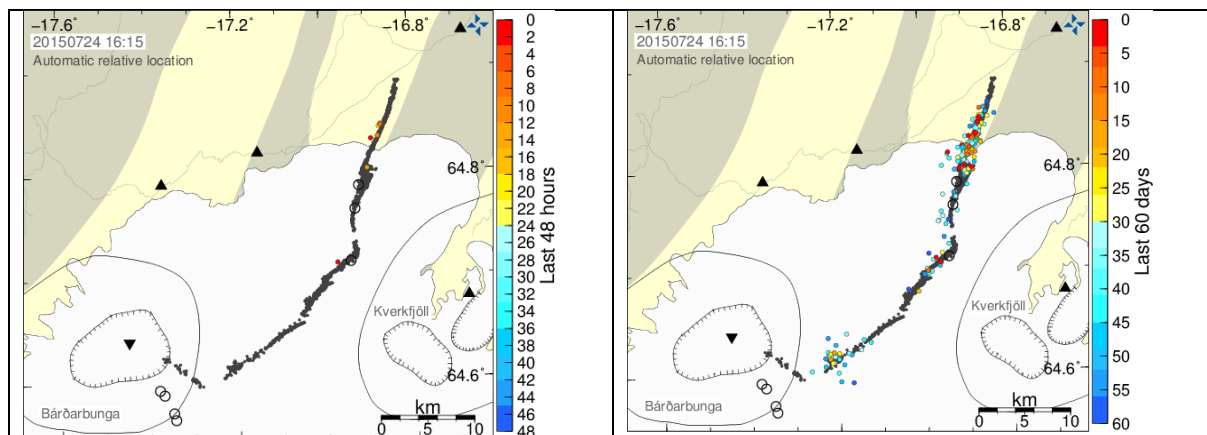


Figure 2.6. Real-time maps from 16:15 on 24 July 2015, displaying the results of the almost near-real-time *ARL* algorithm at Bárdarbunga volcanic system. Black dots represent the previously analyzed library events. (Upper left) Automatic single-event locations in the Bárdarbunga intrusion dyke over the previous 48 hrs. (Upper right) Manually revised events in the Bárdarbunga volcanic system over the previous 60 days. (Lower left) Automatic relative relocations of the automatic earthquakes in the dyke passing the quality criterion over the previous 48 hrs. (Lower right) Automatic relative relocations of earthquakes in the dyke over the previous 60 days.

The development and implementation of the *ARL* procedure will continue until the end of the FUTUREVOLC project. This includes building a more complete event library for the whole Bárdarbunga volcanic system, tuning the parameters to optimum performance and making the necessary changes in the operational environment of the seismic analysis to ensure a decreased processing time, from the present 14 minutes to around 5 minutes like previously attained.

## 2.4 Conclusions

High-precision locations of 4000 earthquakes at Bárdarbunga have mapped out details of the dyke intrusion from August/September 2014. The events form the initial event library required to enable the implementation of automatic, high precision relocations, *ARL* of events in the dyke. Further addition of events from other areas of the volcanic system will enable a more comprehensive mapping of the activity at the volcano. The newest version of the algorithm takes into account the significant depth range of earthquakes at Bárdarbunga. The present operational environment, however, limits the processing speed, but foreseen improvements should enable cutting the processing time down to a few minutes. Fully operational, the *ARL* process can be an important tool for monitoring volcanic activity in near-real time in the event of escalating unrest.

The *ARL* process was tested for activity in the Bárdarbunga dyke intrusion for one month in summer 2015. The testing showed that around 50% of the events that were passed to the *ARL* algorithm were adequately located and that the quality of the locations was sensitive to appropriate library-event coverage. To

improve the coverage of the event library, events from uncovered depth ranges of the dyke as well as from the caldera will be added.

A map has been set up on IMO's web site ([hraun.vedur.is/ja/FUTUREVOLC/BB](http://hraun.vedur.is/ja/FUTUREVOLC/BB)). The map displays *ARL* locations in near-real time showing the activity at Bárðarbunga volcano over the last 48 hours as well as over the last two months (Figure 2.6). The map displays NRT seismic activity in the intrusion dyke and as such can enable real-time monitoring of volcanic activity at Bárðarbunga.

The seismic activity in the Bárðarbunga volcanic system has diminished and the automatic detections are few per day, but the process will continue to function as an early detection of heightened activity and seismicity propagating out of the caldera and into an intrusion.

## 2.5 Acknowledgements

The development work required to adapt the *ARL* earthquake relocation process to the Bárðarbunga volcanic system was heavily supported by the contributions of Ragnar Slunga, the author of the original relative relocation software used.

## 2.6 References

- Böðvarsson, R., S. Th. Rögnvaldsson, S.S. Jakobsdóttir, R. Slunga, R. Stefánsson, (1996). The SIL data acquisition and monitoring system. *Seismol. Res. Lett.*, 67, 35-46.
- Böðvarsson, R., S. Th. Rögnvaldsson, R. Slunga and E. Kjartansson, (1999), The SIL data acquisition system - at present and beyond year 2000, *Phys. Earth Planet. Inter.*, 113, 89–101.
- Got, J. L., J. Fréchet and F. W. Klein, (1994). Deep fault plane geometry inferred from multiplet relative relocation beneath the south flank of Kilauea. *J. Geophys. Res.*, 99, 15375-15386.
- Sigmundsson, F., A. Hooper, S. Hreinsdóttir, K. S. Vogfjörð, B. G. Ófeigsson, E.R. Heimisson, S. Dumont, M. Parks, K. Spaans, G. B. Gudmundsson, V. Drouin, Th. Árnadóttir, K. Jónsóttir, M. T. Gudmundsson, Th. Högnadóttir, H. M. Fridriksdóttir, M. Hensch, P. Einarsson, E. Magnússon, S. Samsonov, B. Brandsdóttir, R. S. White, Th. Ágústadóttir, T. Greenfield, R. G. Green, Á. R. Hjartardóttir, R. Pedersen, R. Bennett, H. Geirsson, P. LaFemina, H. Björnsson, F. Pálsson, E. Sturkell, C. J. Bean, M Möllhoff, A. Braidon, and E P.S. Eibl (2014). Segmented lateral dyke growth in a rifting event at Bárðarbunga volcanic system, Iceland, *Nature*, 517, 191–195, doi:10.1038/nature14111.

Slunga, R., Rögnvaldsson, S. Th., and R. Böðvarsson, (1995). Absolute and relative locations of similar events with application to microearthquakes in southern Iceland. *Geophys. J. Int.* 123, 409-419.

Stefánsson, R., R. Böðvarsson, R. Slunga, P. Einarsson, S.S. Jakobsdóttir, H. Bungum, S. Gregersen, J. Havskov, J. Helme and H. Korhonen (1993), Earthquake prediction research in the South Iceland seismic zone and the SIL project, *Bull. Seism. Soc. Am.*, 83, 696–716.

Vogfjörd, K., S. Rögnvaldsson R. Slunga, J. Morgan, G. Nolet and R. Allen (1999). Propagation of seismicity during the Sept./Oct., 1996 sub-glacial eruption episode near Bárðarbunga volcano, Iceland. 94th Annual meeting of the Seismological Society of America, San Francisco, California, April 1999.

Vogfjörd, K.S., E. Kjartansson, R. Slunga, P. Halldórsson, S. Hjaltadóttir, G.B. Gudmundsson, H. Sveinbjörnsson, S. Ármannsdóttir, B. THorbjarnardóttir and S. Jakobsdóttir (2010). Development and implementation of seismic early warning processes in South-west Iceland, *Icelandic Meteorological Report*, VI 2010-012, pp 83, ISSN 1670-8261.

Vogfjörd, K., Sigurlaug Hjaltadóttir and R. Slunga (2011). Seismic activity and magma movements at Icelandic volcanoes. *Geophysical Research Abstracts Vol. 13*, EGU2011- 13575, EGU General Assembly 2011, Vienna, Austria.

Vogfjörd, K.S., M. Hensch, V. Hjörleifsdóttir and K. Jónsdóttir (2015a). High-precision mapping of seismicity in the last decades at Bárðarbunga volcano, Iceland. *Geophysical Research Abstracts*, Vol. 17, EGU2015-13430-1, 2015 EGU General Assembly, Vienna, Austria 2015.

Vogfjörd, K.S., M. Hensch, G. Gudmundsson and K. Jónsdóttir (2015b). High-Precision Mapping of Seismicity in the 2014 Bárðarbunga Volcanic Episode. *Geophysical Research Abstracts*, Vol. 17, EGU2015-13634-4, 2015 EGU General Assembly, Vienna, Austria 2015.

Vogfjörd, K.S., M. Hensch, K. Jónsdóttir, G. Gudmundsson, V. Hjörleifsdóttir and B. Ófeigsson (2015c). High-precision resolution of the Bárðarbunga 2014 dyke intrusion and caldera subsidence. 26th IUGG General Assembly Prague, Czech Republic, 2015.

Waldhauser, F., and W. L. Ellsworth, 2000. A double-difference earthquake algorithm: Method and application to the northern Hayward Fault, California. *Bull. Seismol. Soc. Am.*, 90, 1353-1368.

Waldhauser, F., and W. L. Ellsworth, 2002. Fault structure and mechanics of the Hayward Fault, California, from double-difference earthquake locations. *Geophys. Res.*, 107, 10.1029/2000JB000084.